Electron-diffraction study of $SbCl_5$-intercalated graphite

Richard K. Mittleman, N. William Parker,* and Albert V. Crewe
The Enrico Fermi Institute, The University of Chicago, 5640 S. Ellis Avenue, Chicago, Illinois 60637
(Received 24 February 1987)

Using high-resolution electron diffraction we have studied the in-plane superlattice structure of stage-2, -3, and -4 antimony pentachloride–intercalated graphite. We used an analytical scanning transmission electron microscope with a microdiffraction resolution of 100 Å. The samples were examined over a wide temperature range (77–295 K) with no indication of any phase change. Two previously unknown long-range superlattices, with structures $(\sqrt{31}\times\sqrt{31})R\pm 8.95°$ and $(\sqrt{19}\times\sqrt{19})R\pm 23.4°$, and unit cells with long-range molecular orientational ordering were found.

INTRODUCTION

Although graphite intercalation has been known for at least 150 years,[1] it has only recently become the subject of scientific investigation. The phenomenon of intercalation has opened the door to a new field in two-dimensional physics with many potential industrial applications. The high degree of structural ordering and quasi-two-dimensionality of pristine graphite constrain an intercalant to assume a similar structure, creating two-dimensional structures out of materials which are normally three dimensional. This constraint along with low free-carrier concentration in room-temperature graphite ($\cong 1\times 10^{-4}$ free carriers/atom) (Ref. 2) coupled with the ability to adjust the intercalant-to-carbon ratio combine to make intercalated graphite an interesting experimental material. The ability to adjust the physical parameters of this material allows the magnetic, electrical, thermal, and phase properties of solid phenomena to be studied in new ways. In addition, the high degree of anisotropy of the graphite can produce variations in these properties with direction by many orders of magnitude (parallel or perpendicular to the graphite c axis).

The c-axis stacking structure and properties of intercalants within the host material were the first novel properties to be studied in intercalated graphite materials. From x-ray,[3,4] electron microscopy studies,[5] and neutron diffraction,[6] it has been found that the intercalant is arranged so as to form layered structures with a constant number of layers of the host between each layer of intercalant. The number of host layers is called the stage number of the composite material. Graphite intercalation compounds (GIC's) of well-defined stage number have been prepared with stage numbers from 1 to 11. These and other studies have shown a sharp phase transition between stages as the intercalant density is varied. This observation led to the Herold-Daumas model, which describes the distribution of intercalant within the graphite.[7] In this model the intercalant is grouped into islands ranging in size from 100 Å to a few micrometers depending on the material. There are islands of intercalant between every pair of graphite layers with each individual island maintaining the proper c-axis spacing relative to other islands. All available data are compatible with the Herold-Daumas model. Until recently there has been little direct evidence to support it. Levi-Setti *et al.*[8] have reported direct imaging of intercalant islands using a focused ion-beam microprobe. Kaluarachchi and Frindt have claimed to have observed the intercalation process taking place in Ag-TiS_2 *in situ* with an electron microscope.[9] Thomas *et al.* studied the electron-microscope lattice fringes of $FeCl_3$ intercalated graphite and observed the discontinuity of intercalant layers and the deformation of the graphite layers.[10]

One of the more interesting properties of GIC's is the highly anisotropic conductivity[11] (high in-plane, much lower parallel to the c axis) which can be achieved.[12,2] In some instances conductivities surpassing that of copper [5.8×10^5 $(\Omega\,\mathrm{cm})^{-1}$] are achieved, as in stage-2 AsF_5 which has a reported in-plane conductivity of 6.2×10^5 $(\Omega\,\mathrm{cm})^{-1}$.[2] Acceptor GIC's, like GIC's in general, are also known for their catalytic properties.[2] The metallic pentahalides generally intercalate into graphite,[13] and form an interesting subset of the acceptor compounds. Antimony pentachloride intercalants are among the most widely studied intercalants for two reasons. The physical properties of this GIC are unlike those of a superposition of the pure materials, and it is one of the most stable intercalants of graphite in air.[14,15] The altered physical properties are not surprising in light of the fact that upon intercalation the molecule undergoes the dissociation reaction:[16,17]

$$3SbCl_5+2e^-\rightarrow 2SbCl_6^-+SbCl_3\ .$$

Unlike some other metallic pentahalide GIC's which undergo this reaction, such as arsenic pentafluoride,[18] it has been reported that for $SbCl_5$ the reaction does not go to completion. There have also been reports that SbC_4^- is present in the intercalated compound. Evidence for the existence of more than one species of intercalant in $SbCl_5$ GIC's comes from a number of different sources. Boolchand *et al.* have used Mössbauer spectroscopy in identifying all four species of antimony chloride.[19] Using the same technique Friedt *et al.*[20] demonstrated a 2:1 ratio between the two ionic states Sb^{5+} and Sb^{3+}. Hwang *et al.* examined energy-dispersive x-ray spectra and electron energy-loss spectra in identifying domains

of $SbCl_3$ and $SbCl_4^-$.[16]

There have been many in-plane structural studies of $SbCl_5$ GIC's using a varety of techniques, frequently producing differing results. Some of the discrepancies may be explained by the differences in experimental methods. There is a discrepancy between x-ray and electron diffraction data in the temperature regime (180–210 K) for stage $n \geq 2$. Roth *et al.*[21] have found that at low temperatures and low electron beam doses ($\cong 3e^-/\text{Å}^2$ sec) the dominant in-plane commensurate superlattice can be changed into an amorphous phase and that the original structure can be recovered by annealing. This commensurate to glass phase change seen at low temperatures using electron microscopy is not in evidence in x-ray studies. There has been recent speculation that some of the properties of $SbCl_5$ GIC's may be different for bulk and thin samples.[22] These two techniques generally use samples that are very different in thickness, a few millimeters for x rays and less than a few thousand angstroms for electron studies. Salamanca-Riba *et al.*[23] have shown that this particular difference between bulk and thin samples is the result of damage caused by the electron beam. The interaction between the electron beam and the sample produces the glass phase, not an inherent difference in the samples.

The most commonly seen in-plane crystalline structure is a $p(\sqrt{7}\times\sqrt{7})R\pm 19.1°$ (Ref. 24) pattern, which is stable from 0 to 425 K.[25] Associated with this structure is an amorphous phase which at ambient temperatures produces isotropic diffuse halos concentric with the origin, $k=0$. On cooling the sample below $\simeq 230$ K this phase coalesces into a weakly incommensurate $b(\sqrt{39}\times\sqrt{39})R\pm 16.1°$. This structure has been correlated with electron micrographs which display a striped pattern with a periodicity of $\simeq 600$ Å.[26] This has been interpreted as evidence for a mass-density wave (MDW) in the intercalant layer produced by a modulated $b(\sqrt{39}\times\sqrt{39})$ structure. Other electron[23,27,28] and x-ray[25,29] diffraction measurements show the $b(\sqrt{39}\times\sqrt{39})$ at ambient temperatures coexisting with the $p(\sqrt{7}\times\sqrt{7})$ structure. As with the $p(\sqrt{7}\times\sqrt{7})$ structure this structure undergoes a transition to a glassy phase around 200 K when exposed to an electron beam.[27] The amount of the $b(\sqrt{39}\times\sqrt{39})$ structure relative to the $p(\sqrt{7}\times\sqrt{7})$ structure seems to depend on sample preparation conditions.[26,30,31]

It has been found that the low-temperature structures of these GIC's are strongly dependent on the rate of cooling.[28,29,32,33] In studying the de Haas–van Alphen (dHvA) oscillations in $SbCl_5$ GIC's it has been found that if the time for cooling room temperature to $\simeq 200$ K is less than 24 h a very complicated dHvA spectra is observed independent of state (1–5). A slower cooling rate produces a very simple dHvA spectra and presumably a simpler in-plane lattice structure.

One theory postulates that upon intercalation the $SbCl_5$ molecule dissociates and forms islands (100–1000 Å) of antimony-rich $SbCl_3$ and $SbCl_4^-$ with a background composed of $SbCl_6^-$ and $SbCl_5$.[16] In this model the islands form a commensurate $(\sqrt{7}\times\sqrt{7})R\pm 19.11°$ lattice and the background is liquidlike in structure at room temperature and coalesces into the $(\sqrt{39}\times\sqrt{39})R\pm 16.1°$ lattice around 200 K. Others have stated that the islands are composed of a close-packed arrangement of $SbCl_6^-$ forming the $(\sqrt{7}\times\sqrt{7})R\pm 19.11°$ lattice.[19,34] In this case the background is composed of $SbCl_3$. It has been suggested that the $SbCl_3$ forms a $(\sqrt{39}\times\sqrt{39})$ lattice by pairing up into an alternating dimer structure with the Cl^- in contact with the bounding graphite layers.[25] Salamanca-Riba *et al.* have used a computer-modeling technique to simulate their electron-microscope micrographs and have determined that the $(\sqrt{7}\times\sqrt{7})$ is composed of a mixture of $SbCl_3$ and $SbCl_6^-$.[23] They also have suggested an electron-beam-activated mechanism for the commensurate-to-glass transition involving the creation of a metastable Cl_2^- and the reaction:

$$SbCl_6^- + SbCl_3 \rightarrow SbCl_5 + SbCl_4^- \ .$$

Suzuki *et al.*[35] have suggested another model based on their work using electron-diffraction, specific-heat, and static susceptibility measurements. They have proposed that the room-temperature compound is composed of two separate phases corresponding to the two dominant species, $SbCl_6^-$ and $SbCl_3$. The majority phase ($SbCl_6^-$) forms a $(\sqrt{7}\times\sqrt{7})$ commensurate lattice which is stable down to 210 K where it changes to a glassy phase. The minority phase ($SbCl_3$) is composed of locally commensurate domains $(\sqrt{7}\times\sqrt{7})$ separated by a regular domain wall structure of discommensurations similar to the low-temperature alkali-metal GIC's.

In addition, some more complicated structures have been observed which have been intepreted in terms of an expansion of the basic $(\sqrt{7}\times\sqrt{7})$ superlattice. Homma and Clarke[25] have reported $b(14\times 14)R0°$ and $b(28\times 28)R0°$ unit-cell structures and interpreted them as being due to alternating dipole directions in $SbCl_3$ having $(\sqrt{7}\times\sqrt{7})$ spacings.

Housar *et al.* have found that $(\sqrt{7}\times\sqrt{7})$ structure is also stable at high pressures (14 kbar) but that the amorphous structure undergoes a phase transition to a very complicated structure at 3 kbar.[34] They have suggested that along with a structural transition the $SbCl_3$ undergoes an angular tilt such that its trigonal axes lie at some angle to the basal plane normal.

METHODS

In this study we investigated stage-2, -3, and -4 antimony pentachloride–intercalated graphite compounds. The samples were prepared by Dr. D. M. Hwang from Bell communications Research Laboratory with highly oriented pyrolytic graphite (HOPG) donated by Union Carbide Corporation and high-purity $SbCl_5$. The standard two-temperature zone method was used and the samples were intercalated gradually over a two-month period to avoid exfoliation and ensure sample homogeneity.[36] To examine the specimens we used a scanning transmission electron microscope at a relatively low voltage of 26 kV. This technique dictated that our samples had to be particularly thin. The mean-free-path length of electrons in amorphous carbon at this energy is about

400 Å for elastic scattering and 260 Å inelastic. The graphite samples were prepared via a variation of the tape and glue method.[16] Specimens were repeatedly frozen between two damp glass slides using dry ice. The slides were then carefully pulled apart, cleaving the graphite into successively thinner sections. By using ice as the "glue," specimen purity was more easily preserved than with the more common sticky-tape methods. Eventually, the graphite was thin enough for use in the scanning transmission electron microscope (<1000 Å). The graphite sections were then suspended in distilled water and scooped up onto a plastic microgrid. This technique ensured that the samples came in contact with distilled water only.

ANALYTICAL SCANNING TRANSMISSION ELECTRON MICROSCOPE

A scanning transmission electron microscope (STEM) which has been developed at the Enrico Fermi Institute was used to gather the data.[37] This STEM was developed as an analytical microscope with a high probe current and has been optimized for analyzing materials. Operating in a medium voltage range up to 50 kV this machine was built to combine flexibility with high performance. It is possible to sequentially image a specimen at high resolution (15–50 Å), probe it in diffraction space with 0.1 $Å^{-1}$ resolution, and to take energy-loss spectra of the transmitted beam with energy resolutions of better than 0.2 eV. Two sets of changeable apertures and three magnetic lenses allow the beam angle, current, and resolution to be adjusted to optimize conditions for the operating mode. The combination of a magnetic lens above the accelerator and eight interchangeable beam defining apertures allows the specimen probe current to be adjusted with relatively little effect on specimen resolution. High resolution can be maintained at very high beam currents (up to $\cong 3\times 10^7 e^-/Å^2\,\text{sec}$); high enough to record a high signal-to-noise ratio diffraction micrograph of a single layer of graphite in a single raster scan (17 sec).

A second magnetic lens between the beam aperture and the objective lens allows the beam angle at the specimen to be adjusted to optimize for the operating mode. This allows diffraction data to be obtained for a range of modes, from convergent to nearly parallel beam angles at the specimen, trading off image resolution for energy and diffraction resolution. In addition, five interchangeable spectrometer apertures allow the collection angle to be adjusted to optimize the spectrometer for any running conditions. The data were gathered at a beam voltage of 26 kV, which resulted in an electron wavelength of 0.076 Å and a Ewald diffraction sphere radius of 83.68 $Å^{-1}$. A liquid-nitrogen Dewar was used to examine the sample behavior as a function of temperature (77–295 K). Two different procedures were used to cool the specimens, the first was to fill the Dewar and let the sample equilibrate to 77 K in 15–30 min. The second procedure which we used was to cool the sample to about 210 K and hold it for 1–2 h at this temperature before continuing the cooling process.

COMPUTER

An interactive computer display system was developed to analyze the diffraction data.[37,38] An IBM 4381-2 mainframe computer was used for computation and a Metheus Omega 500 display system was used for imaging and interaction.[4] The system was developed to facilitate the measurement process in a flexible manner. Subroutines may be written and incorporated in many (computer) languages including *APL*, allowing analysis to be developed interactively. Our goals were to be able to rapidly display the data and improve the signal-to-noise characteristics of the micrographs. Secondly, we wanted to analyze the micrographs, specifically diffraction patterns. To do this, routines were written which use a mouse-driven cursor to input a hypothetical unit cell. The resulting diffraction pattern is then calculated and displayed on the high-resolution monitor as it would be observed in the microscope. This pattern can then be overlayed onto the original data to compare the fit. With the use of modern high-speed computers the many calculations needed to find the structure factors from even very intricate unit cells can be performed, in at most, a matter of minutes. In this way many different and very complicated but physically reasonable unit cells can be rapidly examined until one is found that fits the data satisfactorily.

EXPERIMENTAL RESULTS

Both dark-field imaging and diffraction pattern scans show that the intercalant forms islands of higher density on the order of a few hundred to a few thousand angstroms in size. Our intercalated samples, as determined by transmitted energy loss spectra, were approximately $\cong$400-Å thick (about $1\frac{1}{2}$ inelastic pathlengths in pristine graphite), so we were typically looking at about 30 layers of intercalant. Figure 1(a) shows a micrograph of stage-4 $SbCl_5$ intercalated graphite, at a full scale of 11.2 μm. The elastic and inelastic images of different stage samples were qualitatively indistinguishable. A higher magnification picture of Fig. 1(a) is shown in Fig. 1(b) with a full scale of 2.8 μm. The separation of the intercalant into antimony-rich islands ($SbCl_3 + SbCl_4^-$) and metal-deficient background ($SbCl_5 + SbCl_6^-$) combined with the high collection efficiency of the STEM, leads to very-high-contrast micrographs. The contrast is still much lower than in similar micrographs of alkali-metal GIC's due to the molecular dissociation and relatively smooth distribution of intercalant. The distribution of denser islands is also different from the alkali-metal GIC's. Whereas the islands of intercalated alkali seem to be uniformly distributed with only small density changes near HOPG domain boundaries, the denser areas of $SbCl_x$ ($x=3,4,5,6$) are clustered around the grain boundaries. A closer examination [Fig. 1(b)] reveals the island structure of the intercalant within the graphite domains. Since the specimen thickness was between one and two pathlengths, multiple scattering is apparent and is a significant factor in many areas in the intensity of the intercalant diffraction spots farther out than approximately 3.5–4 $Å^{-1}$. The absence of pro-

nounced Kikuchi[39] lines, however, tells us that we can ignore effects from any scattering of higher than second order.

The diffraction patterns and resulting simulated structures of the intercalant were different in each of the three stages which we studied. Some of these were structures which have not been previously reported in antimony-pentachloride GIC's. Although each of the different stages had different in-plane superlattices, all of the diffraction patterns from "islands" within a single domain showed consistent superlattice orientations. This indicates that regardless of the degree of staging or c-axis correlation the intercalant lattices did have long-range interactions and ordering. Another consistent factor among all of the samples and areas was the overall radial modulation from the molecular structure factor of the intercalant.

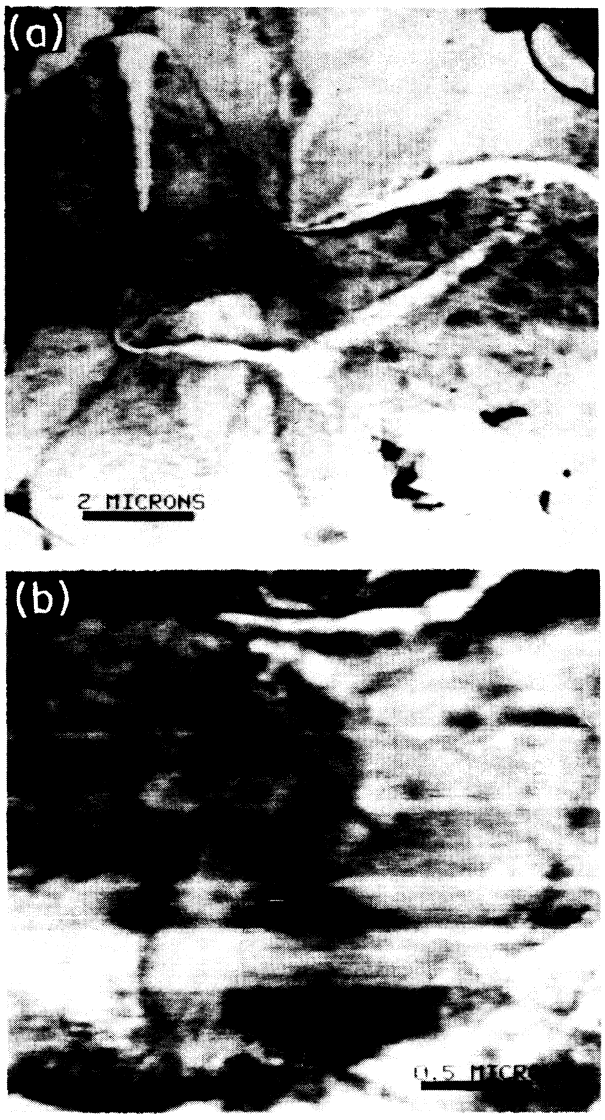

FIG. 1. (a) Dark-field STEM image of stage-4 $SbCl_5$ intercalated graphite (full scale 11.2 μm). (b) Higher magnification image of the same area (full scale 2.8 μm).

The stage-2 samples showed a number of different in-plane structures. One structure which exhibited $(4\times4)R\pm0°$ ordering over a very short range and was seen in conjunction with amorphous rings at 1.3 and 2.03 ± 0.5 Å^{-1}, corresponding approximately to the spacing for close-packed $SbCl_x$. The dominant long-range superlattice structure which was seen in the stage-2 samples was a $(\sqrt{31}\times\sqrt{31})R\pm8.95°$ lattice with amorphous rings at 1.03 and 2.20 ± 0.05 Å^{-1}, which corresponds approximately to a $\sqrt{7}$ nearest-neighbor spacing. Figure 2(a) (±6.4 Å^{-1} full scale) shows an example of this type of pattern. Figure 2(b) illustrates one possible unit cell and its orientation relative to the graphite lattice. This unit cell is the densest possible $SbCl_6^-$ commensurate superlattice possible and is within a few percent of the density of a close-packed arrangement; its chemical formula is $SbCl_5C_{20.7}$. Unlike the $(\sqrt{7}\times\sqrt{7})$ structure, for $SbCl_6^-$ this superlattice does not involve the overlap of the chlorine ionic radii. The separation of molecules in this unit cell is 7.876 Å, which, based on ionic radii, is nearly the diameter of one molecule (7.77 Å). If some multiple scattering, i.e., one graphite and one intercalant interaction, which is consistent with the specimen thickness and finite superlattice (island) size is assumed, then the observed patterns can be fully explained. The more commonly seen $(\sqrt{7}\times\sqrt{7})$ superlattice structure is also seen superimposed on some of these diffraction patterns. Figure 2(c) is a schematic interpretation of the diffraction micrograph of Fig. 2(a) with the size of the dots representing the intensity of the diffraction spots in the original data. The four (+) represent the diffraction spots which are not fit by this model; they are at the same radii as the first- and second-order graphite reflections, but rotated, and are due to another graphite domain. To fully explain these diffraction patterns it is necessary to assume either short-range order along the c-axis with a correlation length of 2–3 layers of intercalant, or a unit cell of 2–3 molecules. A short-range correlation along the c-axis in stage-2 $SbCl_5$ is consistent with the results of Homma and Clarke.[25] A unit cell of three $SbCl_3$ or $SbCl_6^-$ molecules in the symmetry positions of a $(\sqrt{31}\times\sqrt{31})$ unit cell would be 68% as dense as a $(\sqrt{7}\times\sqrt{7})$ superlattice. This is more physically reasonable than the low in-plane density that a single-molecule unit cell on a $(\sqrt{31}\times\sqrt{31})$ lattice would otherwise imply.

Figure 3(a) is a low magnification electron-diffraction (±7.7 Å^{-1} full scale) from the stage-3 sample. The central section of the pattern is shown in Fig. 3(b) (±1.9 Å^{-1} full scale). This sample only exhibited one regular superlattice and amorphous rings. The regular lattice was the commonly seen $(\sqrt{7}\times\sqrt{7})R\pm19.1°$, and the radii of the rings were 1.14 and 1.94 ± 0.08 Å^{-1}. The first-order spots were much more intense than the second-order spots, indicating that the lattice was well ordered only over short ranges (20–40 Å). Strong multiple scattering was observed from a few of the outer graphite reflections, also indicating that the areas of $(\sqrt{7}\times\sqrt{7})$ lattice were very small <100 Å. This might be due to

our high beam current, (*generally* $\cong 10^5 e^-/\text{Å}^2\,\text{sec}$) which according to Roth *et al.* would be enough to disrupt this superlattice. This superlattice was commensurate with the graphite lattice and always exhibited both allowed directions of the superlattice down to a spatial resolution of 100 Å, indicating that the two orientations are spatially correlated. Figure 3(c) shows a unit cell and $(\sqrt{7}\times\sqrt{7})R\pm 19.1°$ lattice which generates the simulated pattern shown in Fig. 3(d). The molecules have no fixed orientation relative to the graphite lattice (or each other).

The stage-4 samples exhibited a much stronger in-plane superlattice. A $(\sqrt{19}\times\sqrt{19})R\pm 23.4°$ superlattice with long-range orientational ordering (only one of the two possible symmetry directions) over areas of many micrometers was observed. Along with this pattern

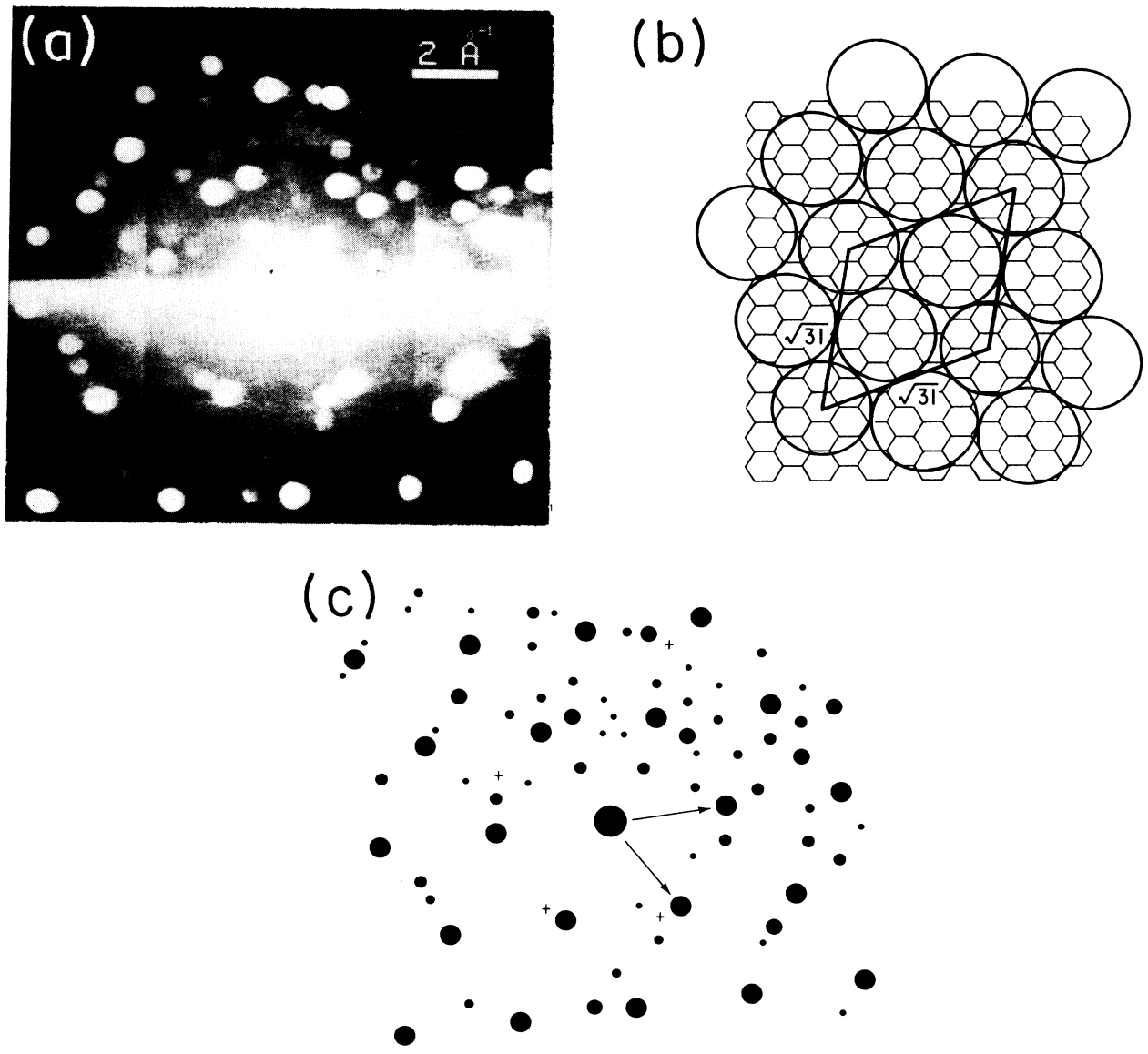

FIG. 2. (a) Diffraction micrograph from stage-2 $SbCl_5$ intercalated graphite (full scale ± 6.4 Å^{-1}). The gain has been reduced in the central portion to prevent saturation. (b) A unit cell which would produce the diffraction pattern of (a). The commensurate lattice vectors are shown $[(\sqrt{31})R\,8.95°]$. The circles are in correct proportion to the graphite lattice for an $SbCl_x$ which is free to rotate about its symmetry axis. (c) Schematic interpretation of (a). The size of the spots is proportional to the intensity of the diffraction spots. The arrows point to two first-order graphite spots at 2.95 Å^{-1}. The (+) represent diffraction spots which do not fit a $(\sqrt{31}\times\sqrt{31})R\,8.95°$ lattice and may be due to scattering from the host in another domain of the HOPG.

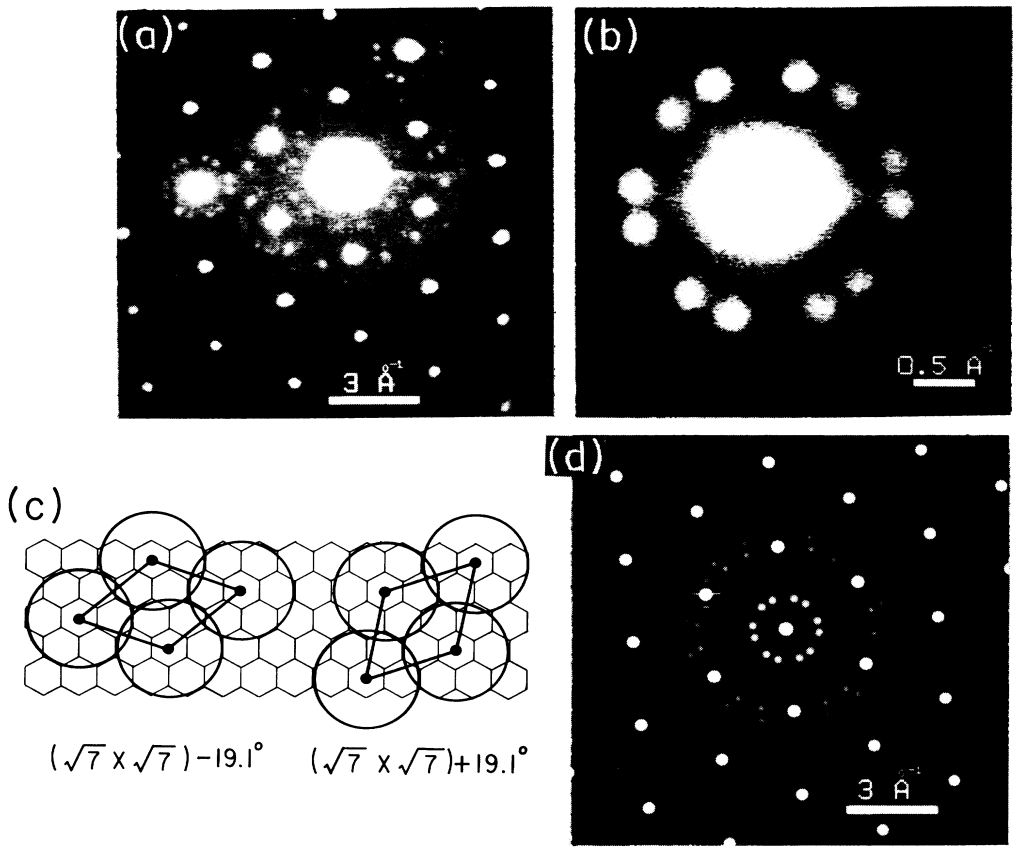

FIG. 3. (a) Diffraction micrograph from stage-3 $SbCl_5$ intercalated graphite (full scale ± 7.7 Å^{-1}). (b) Higher magnification of the central portion of (a) (full scale ± 1.9 Å^{-1}). (c) The two unit cells necessary to produce the diffraction patterns in images (a) and (b). (d) Computer simulation of the diffraction micrograph which would be produced by the superlattices (c). One of the six first-order graphite spots has been circled to the left of the zero-order spot.

there were amorphous rings at 1.15 and 3.01 ± 0.05 Å^{-1}. A small percentage of the diffraction patterns from this sample did not show any orientational ordering, but simply displayed the $p(\sqrt{19} \times \sqrt{19})R \pm 23.4°$ superlattice with only radial modulations. This modulation is due to an average over all rotations of the intercalant molecule about its symmetry axis, or a three-dimensional rotation about the central antimony atom. A computer simulation of this model is shown in Fig. 4. Most areas of the specimen in which we observed the $p(\sqrt{19} \times \sqrt{19})R \pm 23.4°$ structure also showed a modulation characteristic of long-range molecular orientation and/or more than one intercalant molecule per unit cell.

Figure 5(a) (± 3.2 Å^{-1} full scale) is an average of the electron-diffraction micrographs of several successive scans of the same area of the sample. The spots in this pattern are not as highly modulated as most and are closely simulated by a single $SbCl_x$ molecular array with a $p(\sqrt{19} \times \sqrt{19})R\,23.4°$ spacing and orientation as shown in Fig. 5(b). The model we worked from is based on the data of Hwang *et al.* which identified $SbCl_3$ (Ref. 16) as the dominant species in the high-density areas of intercalant. The diffraction pattern resulting from this real-space structure is shown in Fig. 5(c). Figure 6(a) shows a lower magnification-diffraction micrograph (± 6.4 Å^{-1}

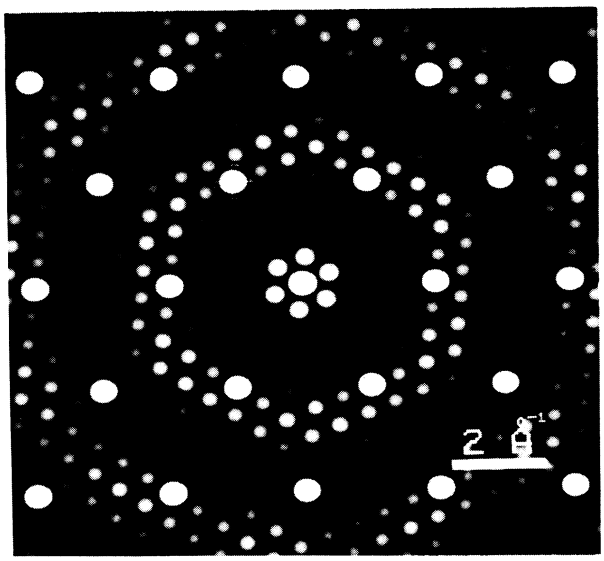

FIG. 4. Computer simulation of $(\sqrt{19} \times \sqrt{19})R\,23.4°$ superlattice of $SbCl_3$ intercalated into graphite with no molecular registration of the intercalant molecules with the graphite lattice. A first-order (100) diffraction spot from the graphite lattice 2.95 Å^{-1} is circled to the top left of the unscattered spot (full scale ± 6.4 Å^{-1}).

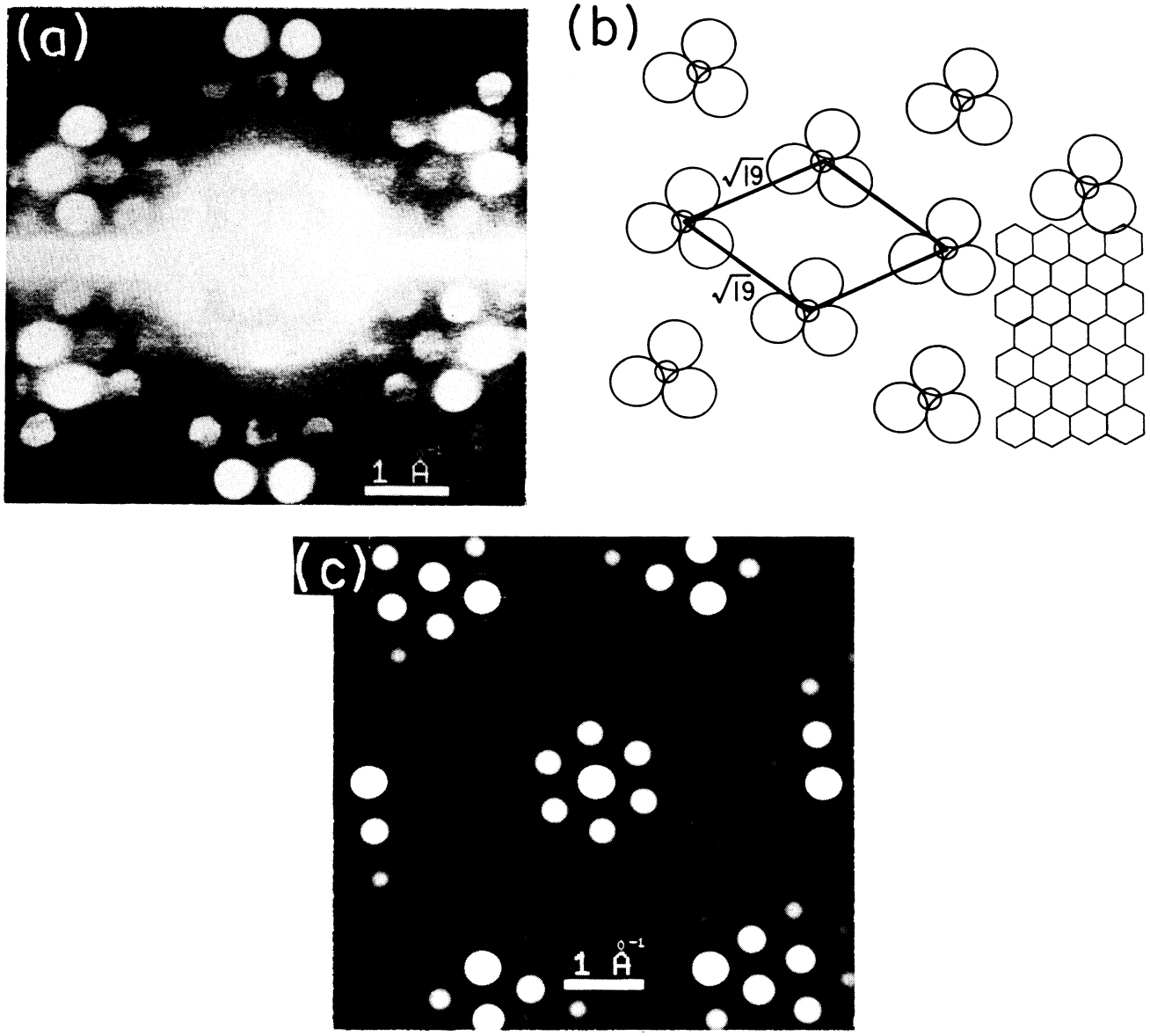

FIG. 5. (a) Diffraction micrograph from stage-4 $SbCl_5$ intercalated graphite (full scale ± 3.2 Å^{-1}). (b) Possible intercalant superlattice to explain image (a). The lattice is a $(\sqrt{19}\times\sqrt{19})R23.4°$ from the graphite lattice with one molecule per unit cell. The large circles represent chlorine and the smaller circles are the antimony. In this schematic the antimony is registered to the center of the graphite hexes in the graphite lattice. A portion of the graphite lattice is shown in the lower right-hand corner. (c) Computer simulation of the diffraction micrograph which would be produced in the analytical STEM by the superlattice of (b). A first-order graphite spot (100) has been circled in the upper left-hand corner.

full scale) from the same sample. This micrograph displays a characteristic, highly modulated pattern of spots around the first-order graphite spots. Figure 6(b) is a $h(\sqrt{19}\times\sqrt{19})R23.4°$ lattice with a basis of 2 with orientational ordering. This structure is similar to the structure of pairs of $SbCl_3$ with alternating c-axis orientation proposed by Homma and Clarke.[25] Using the ionic radii for atomic sizes there is more than enough room within the unit cell and between graphite layers to accommodate this arrangement. This pattern is 74% as dense as the commonly seen $(\sqrt{7}\times\sqrt{7})$ pattern. A very similar simulation is generated by postulating a $(\sqrt{19}\times\sqrt{19})$ in-plane unit cell with a short-range c-axis correlation length (2–3 intercalant layers). The grayscale simulation of this structure is shown in Fig. 6(c). While not an exact match for the data in Fig. 6(a) it is highly suggestive. Figure 7(a) is a diffraction pattern from a nearby area (a different HOPG domain), still rotationally correlated with Fig. 6(a). The pattern is still highly modulated but has a slightly different character. The modulation is smoother, with seven superlattice spots grouped in hexes around the first-order graphite

spots. The best simulations of this data have been achieved by postulating a unit-cell intermediate in density between those shown in Figs. 5(b) and 6(b). Figure 7(b) shows an example of this structure. It has a larger unit cell of $b(\sqrt{76}\times\sqrt{76})R\pm 23.4°$ with a basis of 6. This unit cell is twice as large as the $(\sqrt{19}\times\sqrt{19})$ structure with all of the $\sqrt{19}$ positions filled and two additional molecules. The overlap of the chlorine atoms is permitted due to the trigonal pyramid shape of $SbCl_3$ (Ref. 40) which allows two possible orientations of the trigonal axis relative to the graphite plane. Figure 7(c) is the grayscale simulation created from this superlattice. Overall it is the closest match to the data which we have been able to achieve. While not an exact match, the correlation between Fig. 7(c) and the data is very high. The in-plane molecular density for this structure is 75% as dense as that of the structure in Fig. 6(b) and is 55% as dense as a $(\sqrt{7}\times\sqrt{7})$ superlattice.

All of the samples were examined from ambient to liquid-nitrogen temperature. Our cooling rate was fast compared to the gradual rate found necessary to let the phase change go to completion in the de Haas–van Alphen studies.[28,29,32] We did, however, expect to see some signs of a phase change. Unlike many previous studies, we did not observe any phase changes or any other temperature-dependent effects in any of the samples or various structures. Despite maintaining the samples at various temperatures for extended periods of time

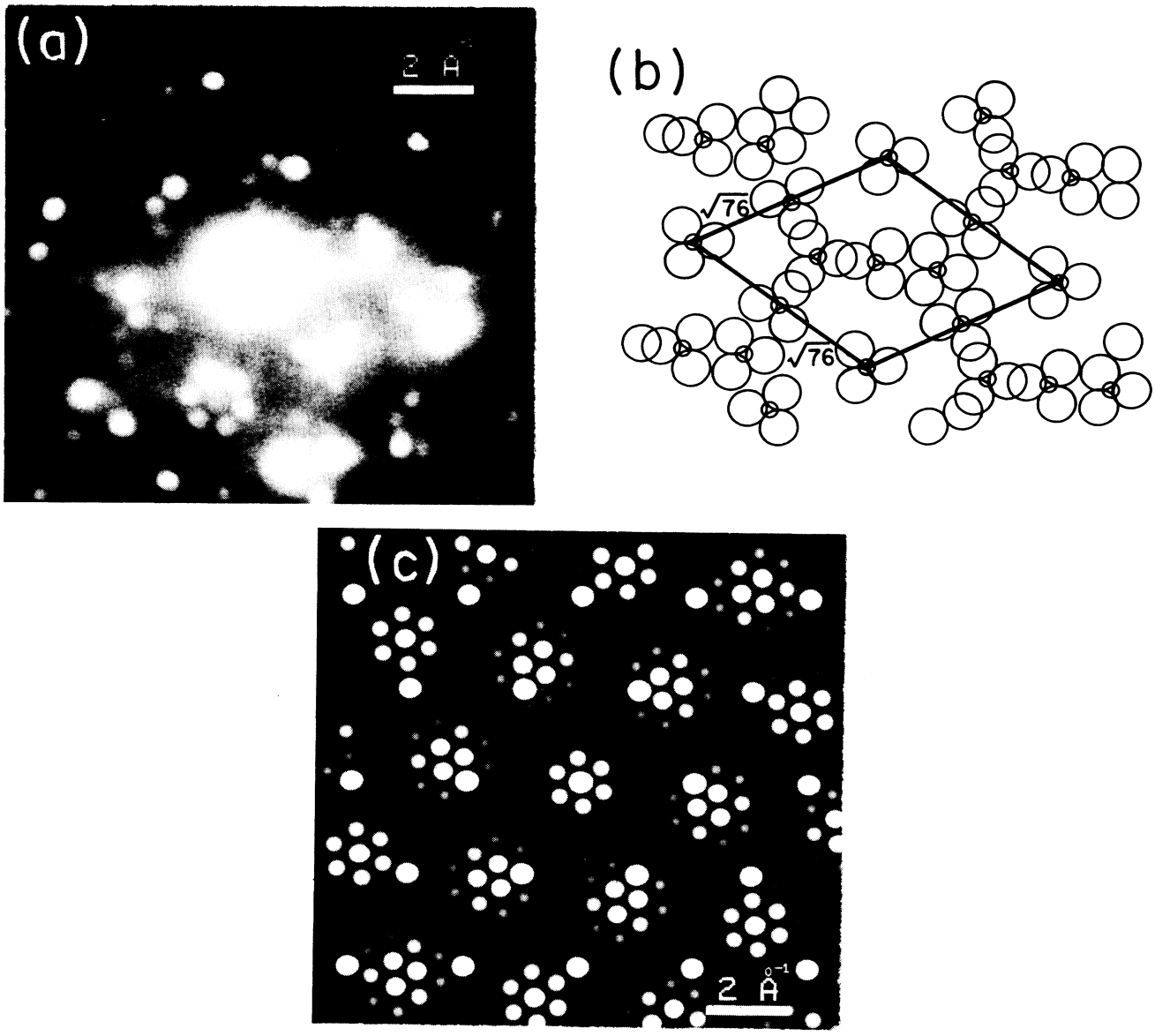

FIG. 6. (a) Diffraction micrograph from stage-4 $SbCl_5$ intercalated graphite (full scale ± 6.4 Å^{-1}). (b) Possible intercalant superlattice to explain (a). The lattice is a $(\sqrt{76}\times\sqrt{76})R23.4°$ from the graphite lattice with six molecules per unit cell. (c) Computer simulation of the diffraction micrograph which would be produced by the superlattice of (b). A first-order graphite spot (2.95 Å^{-1}) has been circled above and to the left of the central spot.

the only temperature dependence present was a nucleation of the already present superlattices at low temperatures.

CONCLUSIONS

We have used electron-beam microdiffraction techniques to study three different stages of antimony-pentachloride–intercalated graphite. The purpose of this work was to study the in-plane structure of the intercalant in the host material on scales under 100 Å. Our samples were derived from HOPG, but since the resolution of our machine and the intercalant "island" sizes are much smaller than the typical domain size (tens of micrometers) of HOPG, our results should be indicative of single-crystal graphite. This is substantiated by our electron-diffraction patterns which, in general, show only one orientation of the graphite lattice.

Our observations clearly support the Herold-Daumas model of intercalation and the direct observation ion-microprobe studies. The real-space micrographs show islands of high contrast within the graphite. The diffraction data was very sensitive to the position of the beam on the specimen with rapid changes from an intercalant superlattice to background scattering and amorphous rings as the beam was moved over the specimen.

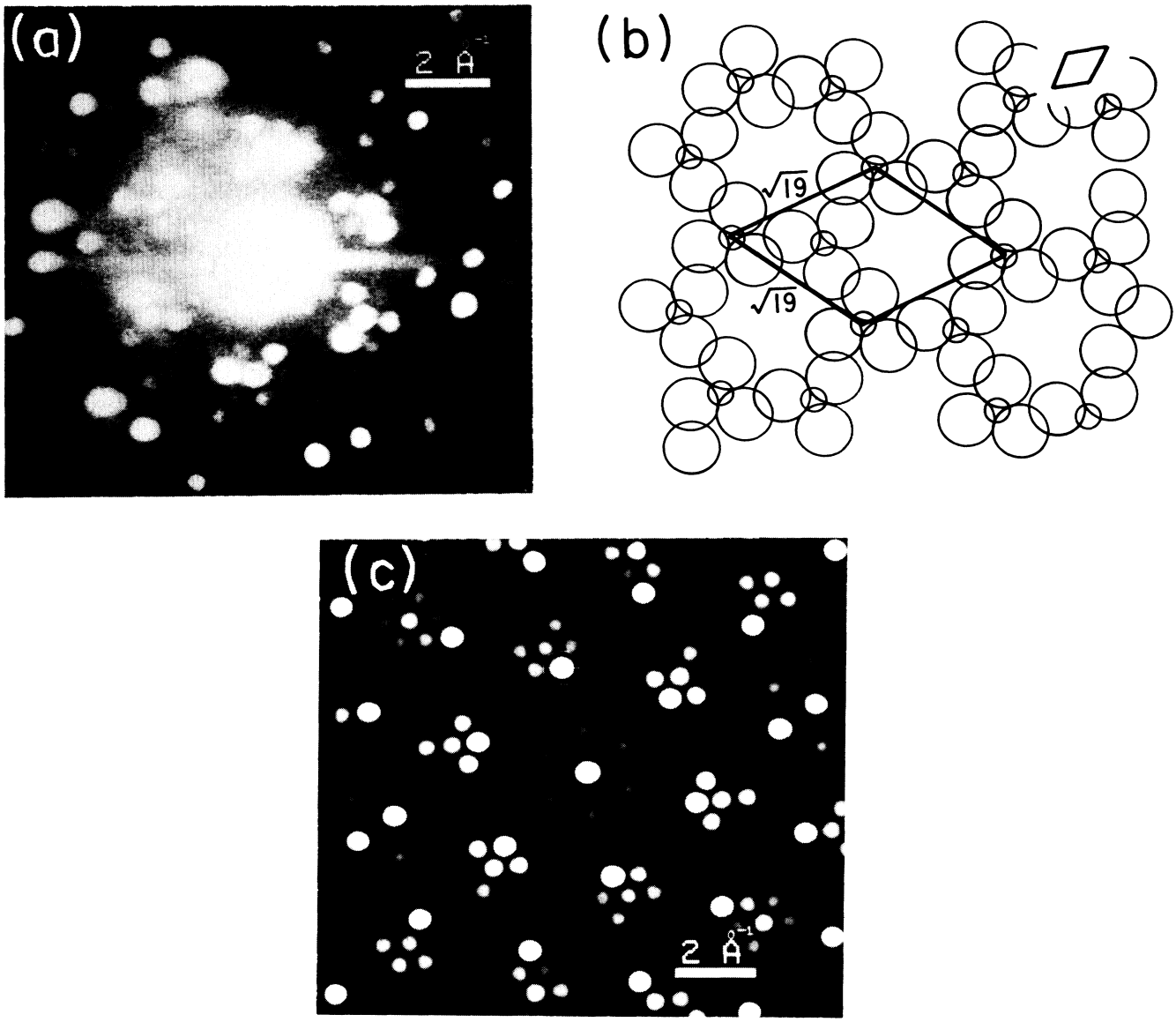

FIG. 7. (a) Diffraction micrograph from stage-4 $SbCl_5$ intercalated graphite (full scale ± 6.4 Å^{-1}). (b) Possible intercalant superlattice to explain (a). The lattice is a $(\sqrt{19}\times\sqrt{19})R23.4°$ from the graphite lattice with two molecules per unit cell. A graphite unit cell is shown in the inset at the upper right-hand corner. (c) Computer simulation of the diffraction micrograph which would be produced by the superlattice of (b). A first-order graphite spot (2.95 Å^{-1}) has been circled above and to the left of the central spot.

Without a tilt stage and thus using diffraction data only from a beam parallel to the c axis it is difficult to reconstruct the full three-dimensional structure of the intercalant. Making use of intensity variations in the diffraction micrographs and the physical parameters of the system, we can create computer simulations of many different physically reasonable structures. Using this procedure, we found that it was not necessary for there to be any c-axis correlations at all to explain our diffraction data. We cannot rule out short-range correlations of less than 3–4 layers. The k vector for the electron beam at which we operated at was 83.68 $Å^{-1}$. Any three-dimensional correlations longer than a few layers would cause radial modulations in the diffraction pattern as the Ewald sphere leaves the zero-order plane in diffraction space. Our diffraction data show no such modulations and therefore limit any possible three-dimensional ordering to at most a few layers. Interpretation is further complicated by the dissociation and possible segregation of $SbCl_5$ into multiple species and phases. A superlattice of $SbCl_6^-$ implies an $A\alpha A$ sandwich stacking (two graphite planes aligned to each other surrounding one intercalant layer[27]). This is caused by the graphite layer moving into registration with the molecular structure of the chlorine ions, so that the ions fit into the holes in the graphite lattice. A superlattice of $SbCl_3$ can have either stacking $A\alpha B$ or $A\alpha A$ depending on the unit cell of the intercalant. This freedom is a result of the dipole nature of $SbCl_3$ which will cause it to alternate in orientation, with the chlorine atoms registering to alternating graphite layers.[41] An $A\alpha B$ stacking (two graphite planes offset relative to each other surrounding one intercalant layer) would align the anitmony atom with a carbon atom in the graphite lattice. In the dipole model this separation is over 3 Å and seems reasonable.

The superlattice structures and their behavior were different from any that have previously been described by other researchers. The two new superlattices $(\sqrt{19}\times\sqrt{19})R\pm23.4°$ and $(\sqrt{31}\times\sqrt{31})R\pm8.95°$ have not been previously observed. We did not observe any temperature dependence over the range which we operated in (77 to 295 K). Specifically, there was no evidence of the phase change in the neighborhood of 230 K which has been observed previously by many others. The commonly seen $(\sqrt{39}\times\sqrt{39})R\pm16.1°$ superlattice was not observed at all. The appearance of the micrograph shown in Fig. 1 was characteristic of the sample at all temperatures with no signs of the striped appearance which Clarke *et al.*[26] associated with a weakly incommensurate superlattice. The angular modulations of the diffraction patterns from the stage-4 sample are not compatible with the rotating-paired dimer model of Homma and Clarke, which predicts a diffraction pattern displaying all of the diffraction spots from the unit cell modulated only by a radial structure factor function and the atomic angular scattering factors. The strongly modulated intensity of the diffraction spots in our micrographs indicates a unit cell where the positions of the atoms in the molecule have not been averaged out, indicating that the intercalant molecules are orientationally locked to the graphite lattice. One possible reason why this has not been seen in previous work might be that this is the first work with sufficient spatial resolution ($\lesssim 200$ Å). Although we were not able to find a unit cell which exactly simulates the data, we were able to find an approximate structure and propose a tentative in-plane molecular density for this structure of one molecule per 1.3×10^{-2} $Å^2$, or $SbCl_xC_{25.3}$. Our data from the stage-2 sample was not incompatible with this model, needing only molecules in the proper positions or stackings with random orientation to fully explain it.

Each stage totally different in-plane superlattice structures. This could imply that the in-plane structure is very sensitive to c-axis density or alternatively that many different superlattices can form during the initial intercalation process and then act as "seeds" which the superlattice nucleates around. All of the samples have in-plane structures which were coherent and commensurate over large areas (many micrometers), confirming the strong nature of the interaction between the intecalant and host material.

Despite careful sample preparation to ensure stage homogenity and equilibrium conditions in the samples it is apparent that the in-plane structure has many different possible commensurate structures which are stable. These different structures are formed in the initial intercalation process and in light of their long-range nature must be caused by the initial conditions. For commercial or scientific purposes one would perfer a uniform, easily controllable material, not one which can form numerous different structures with small changes in preparation conditions. The usefulness of GIC's, experimental or industrial, can not be discarded on this basis since it is likely that many of the physical properties depend only on the density and type of the intercalant and not on the detailed in-plane structure.

ACKNOWLEDGMENTS

We thank M. Utlaut, W. Mankawich, E. Kritchman, and the University of Chicago Division of Physical Sciences Central Shop for substantial efforts during the initial development phase of the microscope. We are grateful to Dr. D. M. Hwang for providing us with the samples and valuable discussion. The data analysis could not have been completed without the contributions of Guy McNamara to the imaging system. We wish to thank IBM for their cooperation in the use of the 4381 system and Metheus Corp. for the donation of the Metheus 500 image display and storage system. Project funding was supplied under National Science Foundation Contract No. DMR8513954 and Department of Energy of Energy Contract No. DEAC0276EV02398 and Contract No. DEFG0286ER60437.

*Present address: MicroBeam, Inc. 1125 Business Center Dr., Newbury Park, CA 91320.
[1]J. E. Fisher and T. E. Thompson, Phys. Today **31**(7), 36 (1978).
[2]M. S. Dresselhaus and G. Dresselhaus, Adv. Phys. **30**, 139 (1981).
[3]U. Hoffmann and A. Frenzel, Z. Elektrochem. **37**, 613 (1931).
[4]A. Schleede and M. Wellmann, Z. Phys. Chem. **18**, 1 (1932).
[5]J. M. Thomas and G. R. Millward, Mater. Res. Bull. **15**, 677 (1980).
[6]W. D. Ellenson, D. Semmingson, D. Guerard, D. G. Onn, and J. E. Fisher, Mater. Sci. Eng. **31**, 137 (1977).
[7]J. Melin and A. Herold, C. R. Acad. Sci. **269**, 877 (1969).
[8]R. Levi-Setti, G. Crow, Y. L. Wang, N. W. Parker, and R. K. Mittleman, Phys. Rev. Lett. **54**, 2615 (1985).
[9]D. Kaluarachchi and R. F. Frindt, Phys. Rev. B **28**, 3663 (1983).
[10]J. M. Thomas, G. R. Millward, R. F. Schlogl, and H. P. Boehm, Mater. Res. Bull. **15**, 671 (1980).
[11]*Physics and Chemistry of Materials with Layered Structures,* edited by J. E. Fisher and F. Levy (Reidel, Dordrecht, 1979), Vol. 6, p. 481.
[12]T. E. Thompson, E. M. McCarron, and N. Bartlett, Synth. Met. **3**, 251 (1981).
[13]M. S. Dresselhaus and G. Dresselhaus, Adv. Phys. **30**, 139 (1981).
[14]V. R. K. Murthy, D. S. Smith, and P. C. Eklund, Mater. Sci. Eng. **49**, 455 (1982).
[15]J. Melin and A. Herold, Carbon **13**, 357 (1975).
[16]D. M. Hwang, X. W. Qian, and S. A. Solin, Phys. Rev. Lett. **53**, 1473 (1984).
[17]N. Bartlett, B. McQuillan, and A. S. Robertson, Mater. Res. Bull. **13**, 1259 (1978).
[18]N. Bartlett, R. N. Biagioni, B. W. McQuillan, A. S. Robertson, and A. C. Thompson, J. Chem. Soc. Chem. Commun. **5**, 200 (1978).
[19]P. Boolchand, W. J. Bresser, D. McDaniel, and K. Sisson, State Commun. **40**, 1094 (1981).
[20]J. M. Friedt, R. Poinsot, and L. Soderholm, Solid State Commun. **49**, 223 (1984).
[21]G. Roth, L. Salamanca-Riba, A. R. Kortan, G. Dresselhaus, and R. J. Birgeneau, in *Graphite Intercalation Compounds,* Material Research Society Extended Abstracts, edited by P. C. Ekland, M. S. Dresselhaus, and G. Dresselhaus (MRS, Pittsburgh, 1984), p. 158.
[22]W. Jones, P. Korgul, R. Schlogl, and J. M. Thomas, J. Chem. Soc. Chem. Commun. **8**, 468 (1983).
[23]L. Salamanca-Riba, G. Roth, J. M. Gibson, A. R. Kortan, G. Dresselhaus, and R. J. Birgeneau, Phys. Rev. B **33**, 2738 (1986).
[24]This notation refers to a traingular superlattice [*p* for close packed, *h* for honeycombed (hexagonal), *b* for other unit-cell bases, and *o* for oblique] commensurate with the graphite lattice and a unit-cell square root of seven times larger than that of graphite ($\sqrt{7}\times 2.46$ Å$=6.51$ Å), rotated 19.1° from the graphite lattice.
[25]H. Homma and R. Clarke, Phys. Rev. B **31**, 5865 (1985).
[26]R. Clarke, M. Elzinga, H. Homma, D. T. Morelli, M. J. Winokur, and C. Uher, Phys. Rev. B **26**, 5250 (1982).
[27]G. Timp, M. S. Dresselhaus, L. Salamanca-Riba, A. Erbil, L. W. Hobbs, G. Dresselhaus, P. C. Eklund, and Y. Iye, Phys. Rev. B **26**, 2323 (1982).
[28]Y. Yosida, S. Tanuma, S. Takagi, and K. Soto, in *Graphite Intercalation Compounds,* Material Research Society Extended Abstracts, edited by P. C. Ekland, M. S. Dresselhaus, and G. Dresselhaus (MRS, Pittsburgh, 1984), p. 51.
[29]H. Zaleski, P. K. Ummat, and W. R. Datars, Phys. Rev. B **35**, 2958 (1987).
[30]M. Suzuki, N. Tanuma, S. Tagaki, and K. Sato, in *Graphite Intercalation Compounds,* edited by Sei-ichi Tanuma and Hiroshi Kamimura (World Publishing, Singapore, 1984), p. 57.
[31]G. Timp, M. S. Dresselhaus, L. Salamanca-Riba, A. Erbil, L. W. Hobbs, G. Dresselhaus, P. C. Ekland, and Y. Iye, Phys. Rev. B **26**, 2323 (1982).
[32]H. Zaleski, P. K. Ummat, and W. R. Datars, J. Phys. C **17**, 3167 (1984).
[33]Y. Yosida and H. S. Tanuma, J. Phys. Soc. Jpn. **54**, 701 (1985).
[34]B. Housar, H. Homma, and R. Clarke, Phys. Rev. B **30**, 4802 (1984).
[35]M. Suzuki, R. Inada, H. Ikeda, S. Tanuma, K. Suzuki, and M. Ichihara, J. Phys. Soc. Jpn. **53**, 3052 (1984).
[36]D. M. Hwang and G. Nicolaides, Solid State Commun. **49**, 483 (1984).
[37]N. W. Parker, R. K. Mittleman, and A. V. Crewe, Rev. Sci. Instrum. **58**, 174 (1987).
[38]G. R. McNamara, O. H. Kapp, and A. V. Crewe, in Proceedings of the 13th International Congress of Biochemistry, Amsterdam, 1985 (unpublished).
[39]T. B. Rymer, *Electron Diffraction* (Methuen, London, 1970).
[40]R. W. G. Wyckoff, *Crystal Structures-Inorganic Compounds,* 2nd ed. (Interscience, New York, 1964), pp. 65–67.
[41]R. Clarke and H. Homma, in *Proceedings of the MRS Symposia on Intercalated Graphite* (Elsevier, New York, 1982), Vol. 20.

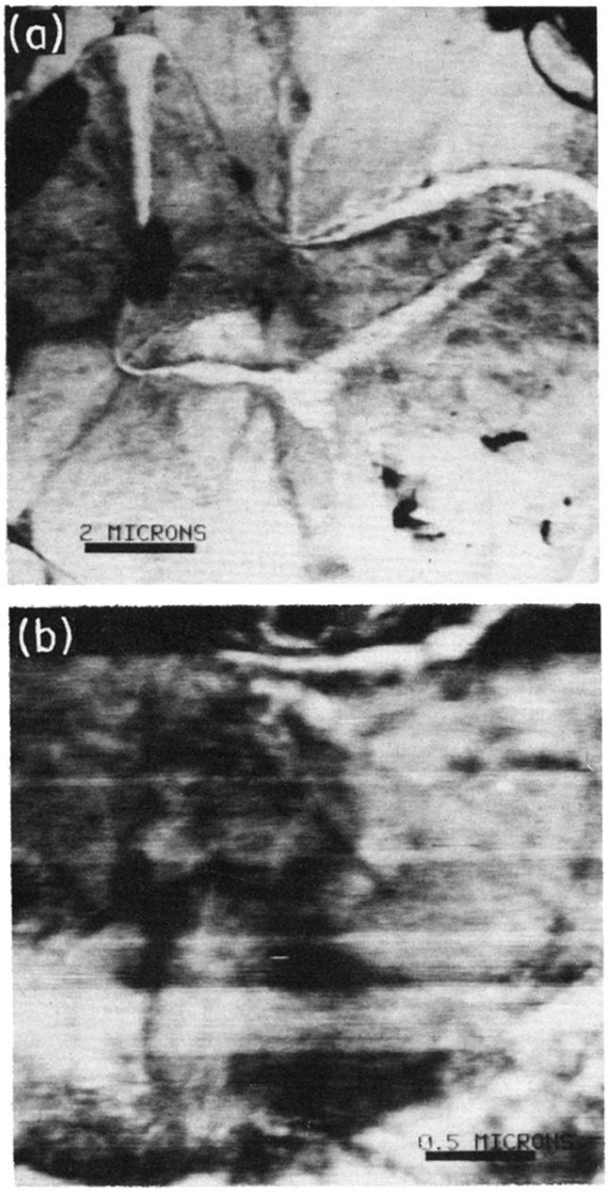

FIG. 1. (a) Dark-field STEM image of stage-4 $SbCl_5$ intercalated graphite (full scale 11.2 μm). (b) Higher magnification image of the same area (full scale 2.8 μm).

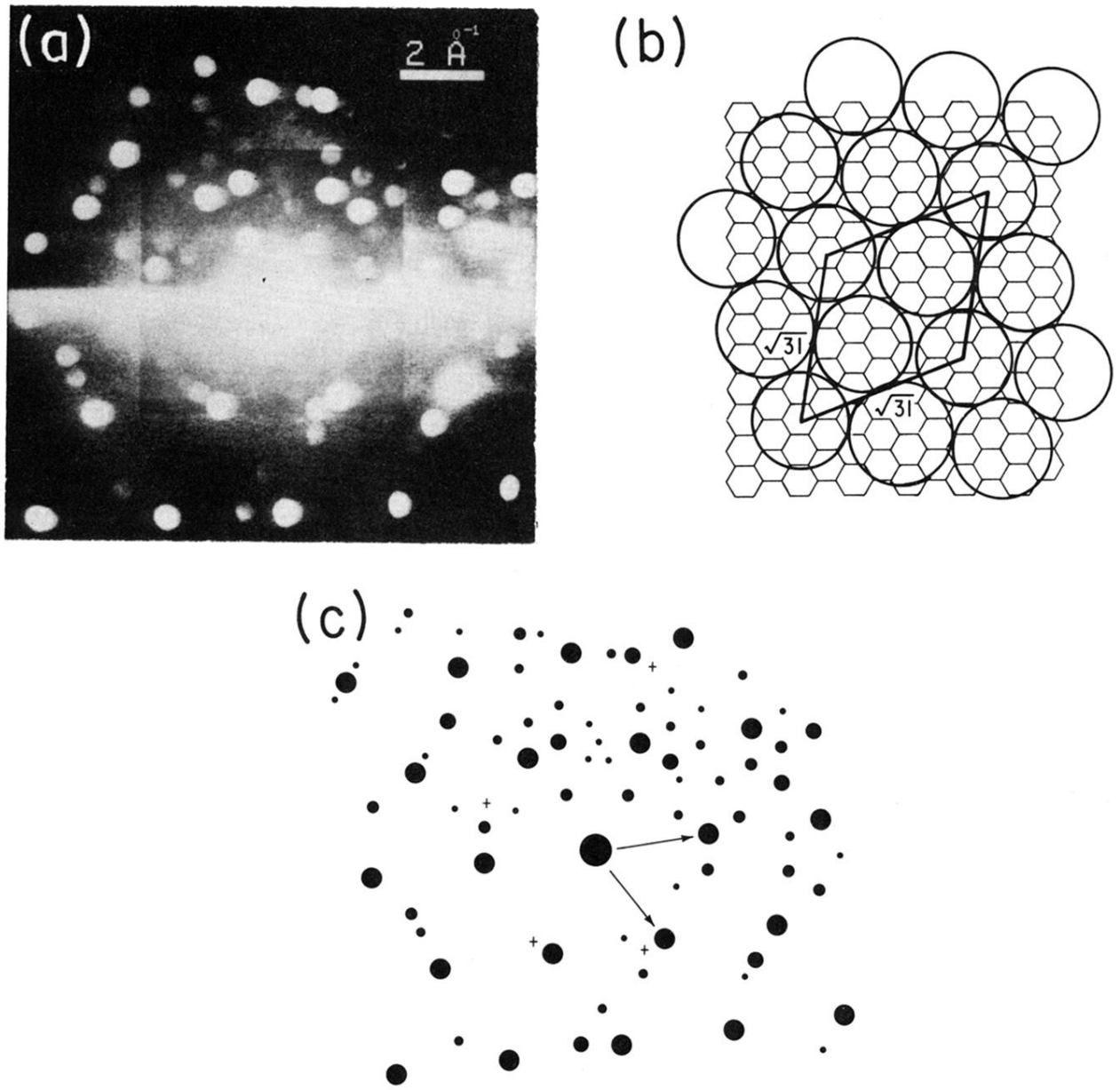

FIG. 2. (a) Diffraction micrograph from stage-2 $SbCl_5$ intercalated graphite (full scale ± 6.4 Å^{-1}). The gain has been reduced in the central portion to prevent saturation. (b) A unit cell which would produce the diffraction pattern of (a). The commensurate lattice vectors are shown [$(\sqrt{31})R\,8.95°$]. The circles are in correct proportion to the graphite lattice for an $SbCl_x$ which is free to rotate about its symmetry axis. (c) Schematic interpretation of (a). The size of the spots is proportional to the intensity of the diffraction spots. The arrows point to two first-order graphite spots at 2.95 Å^{-1}. The (+) represent diffraction spots which do not fit a $(\sqrt{31}\times\sqrt{31})R\,8.95°$ lattice and may be due to scattering from the host in another domain of the HOPG.

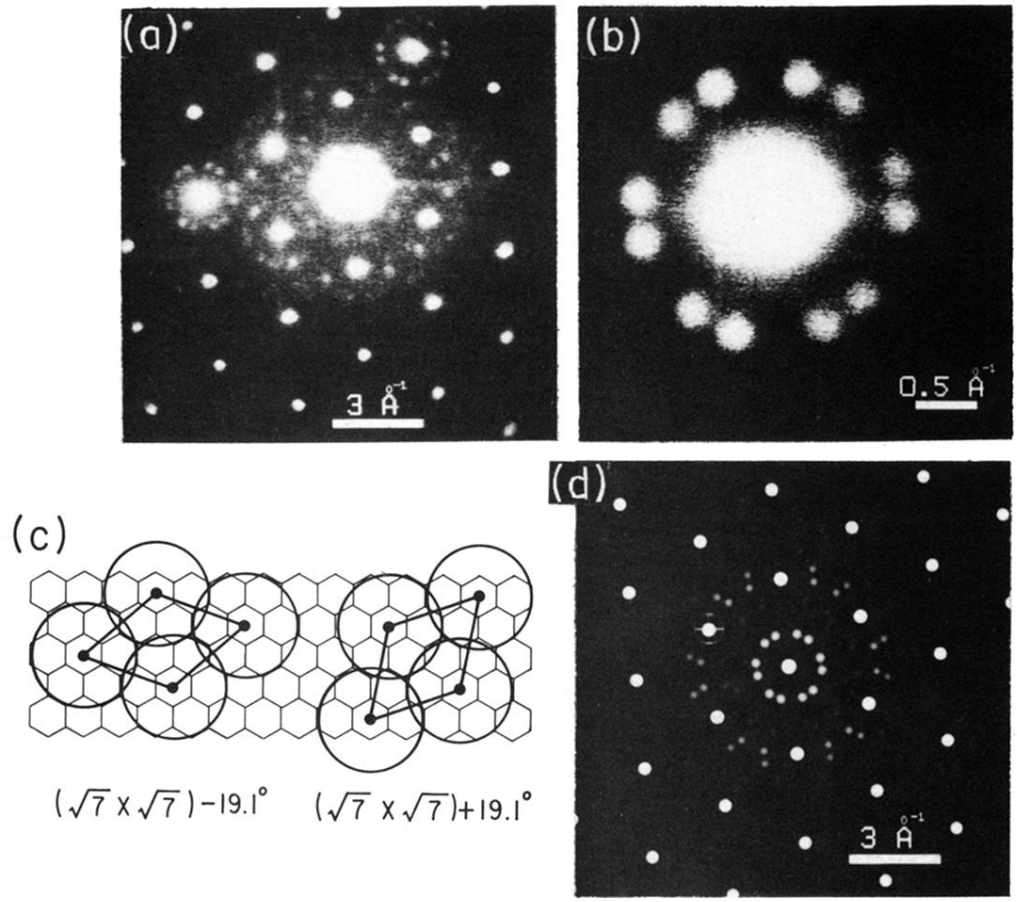

FIG. 3. (a) Diffraction micrograph from stage-3 $SbCl_5$ intercalated graphite (full scale ± 7.7 $Å^{-1}$). (b) Higher magnification of the central portion of (a) (full scale ± 1.9 $Å^{-1}$). (c) The two unit cells necessary to produce the diffraction patterns in images (a) and (b). (d) Computer simulation of the diffraction micrograph which would be produced by the superlattices (c). One of the six first-order graphite spots has been circled to the left of the zero-order spot.

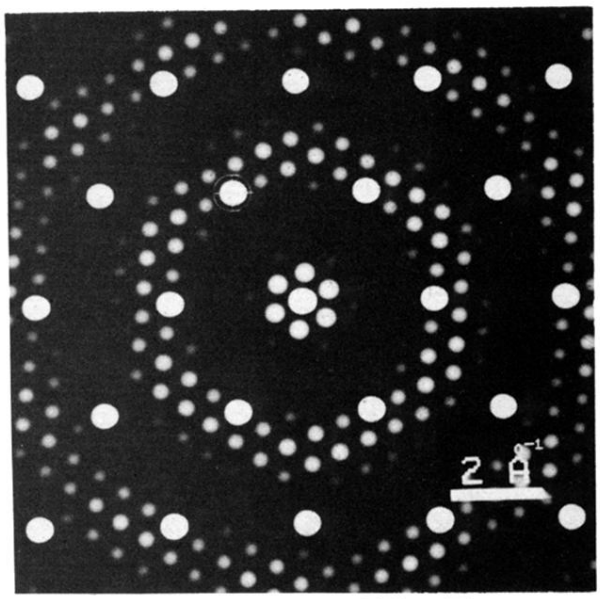

FIG. 4. Computer simulation of $(\sqrt{19}\times\sqrt{19})R23.4°$ superlattice of $SbCl_3$ intercalated into graphite with no molecular registration of the intercalant molecules with the graphite lattice. A first-order (100) diffraction spot from the graphite lattice 2.95 $Å^{-1}$ is circled to the top left of the unscattered spot (full scale ± 6.4 $Å^{-1}$).

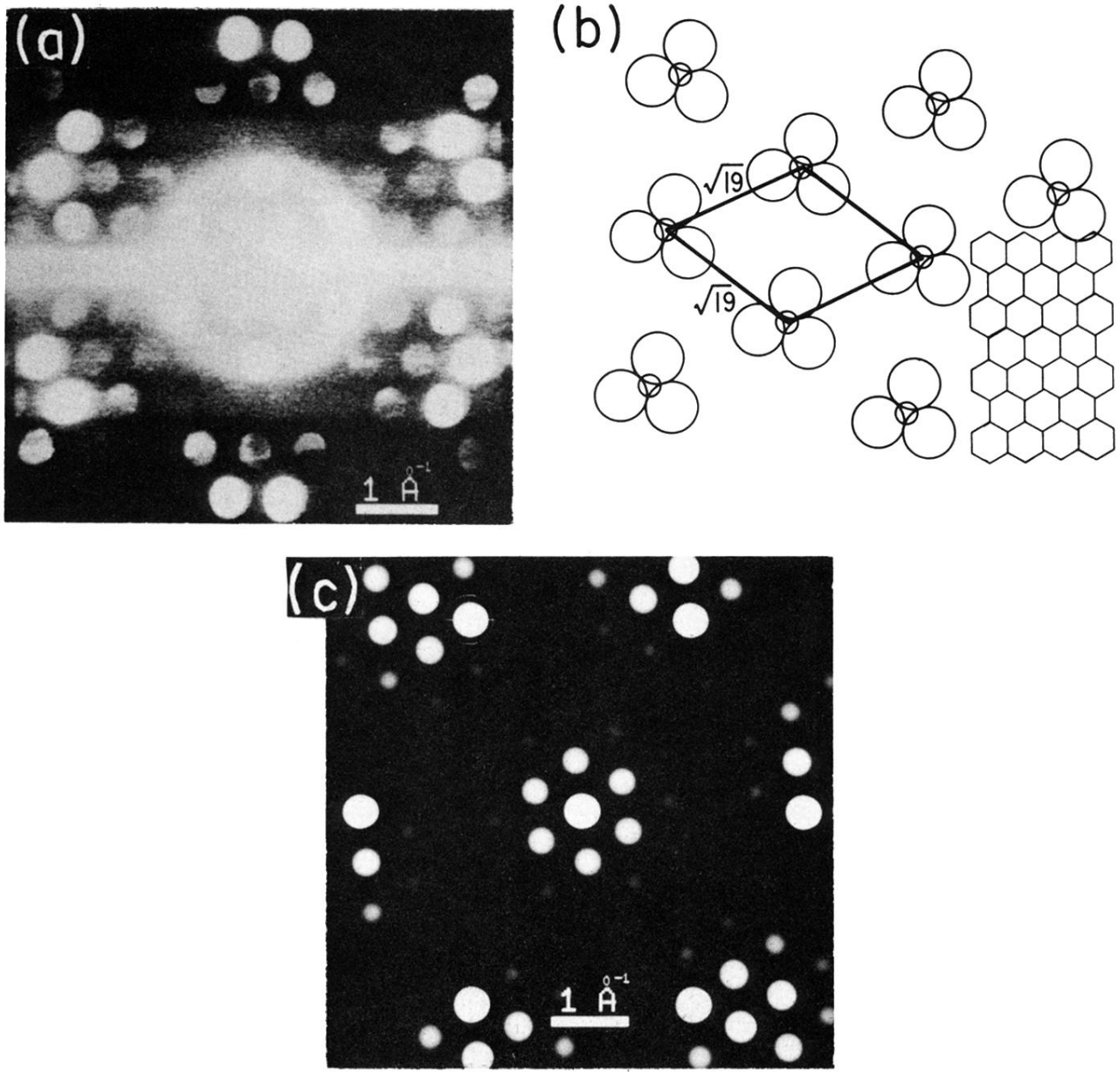

FIG. 5. (a) Diffraction micrograph from stage-4 $SbCl_5$ intercalated graphite (full scale ± 3.2 Å^{-1}). (b) Possible intercalant superlattice to explain image (a). The lattice is a $(\sqrt{19}\times\sqrt{19})R23.4°$ from the graphite lattice with one molecule per unit cell. The large circles represent chlorine and the smaller circles are the antimony. In this schematic the antimony is registered to the center of the graphite hexes in the graphite lattice. A portion of the graphite lattice is shown in the lower right-hand corner. (c) Computer simulation of the diffraction micrograph which would be produced in the analytical STEM by the superlattice of (b). A first-order graphite spot (100) has been circled in the upper left-hand corner.

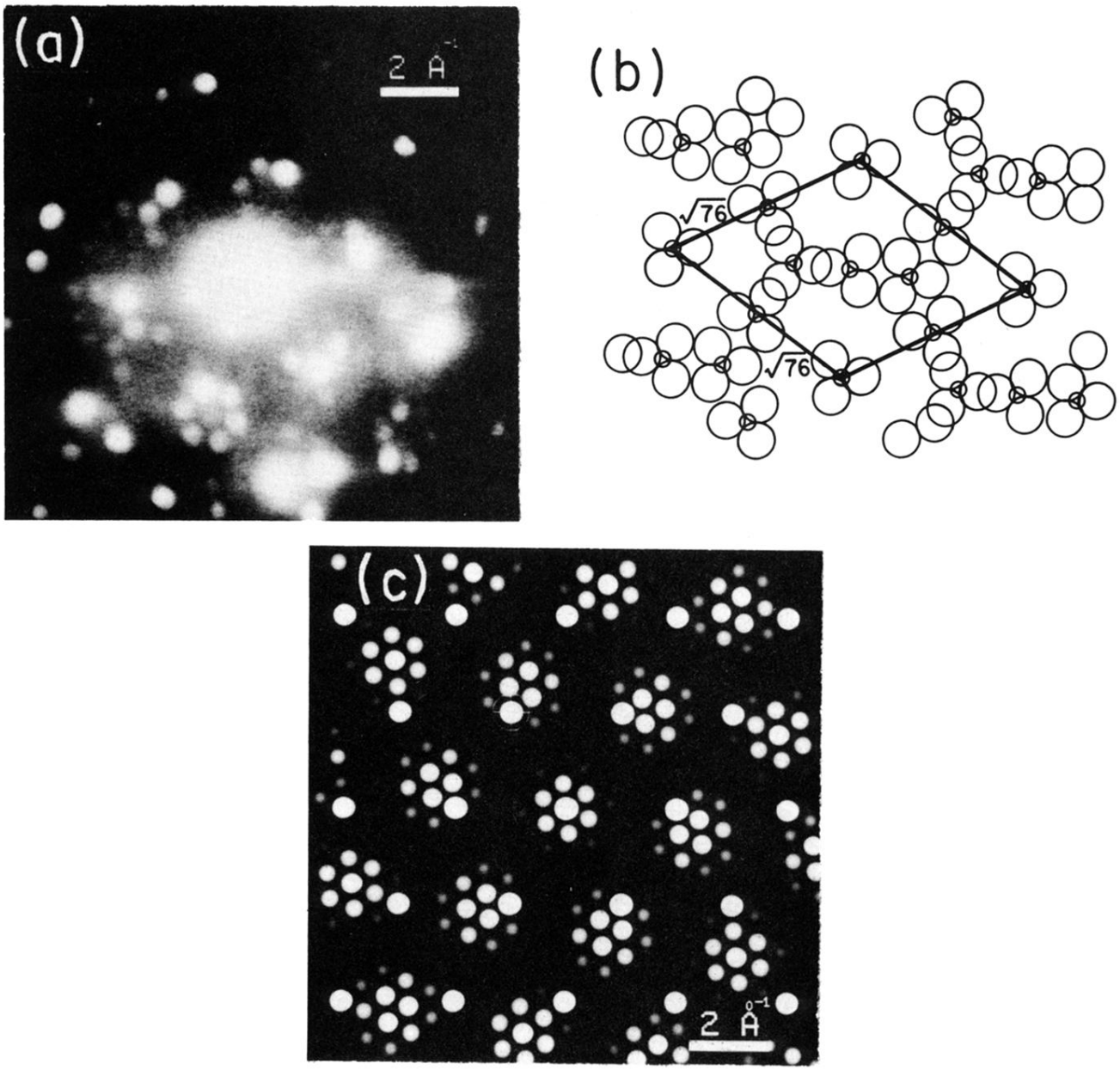

FIG. 6. (a) Diffraction micrograph from stage-4 $SbCl_5$ intercalated graphite (full scale ± 6.4 Å^{-1}). (b) Possible intercalant superlattice to explain (a). The lattice is a $(\sqrt{76}\times\sqrt{76})R23.4°$ from the graphite lattice with six molecules per unit cell. (c) Computer simulation of the diffraction micrograph which would be produced by the superlattice of (b). A first-order graphite spot (2.95 Å^{-1}) has been circled above and to the left of the central spot.

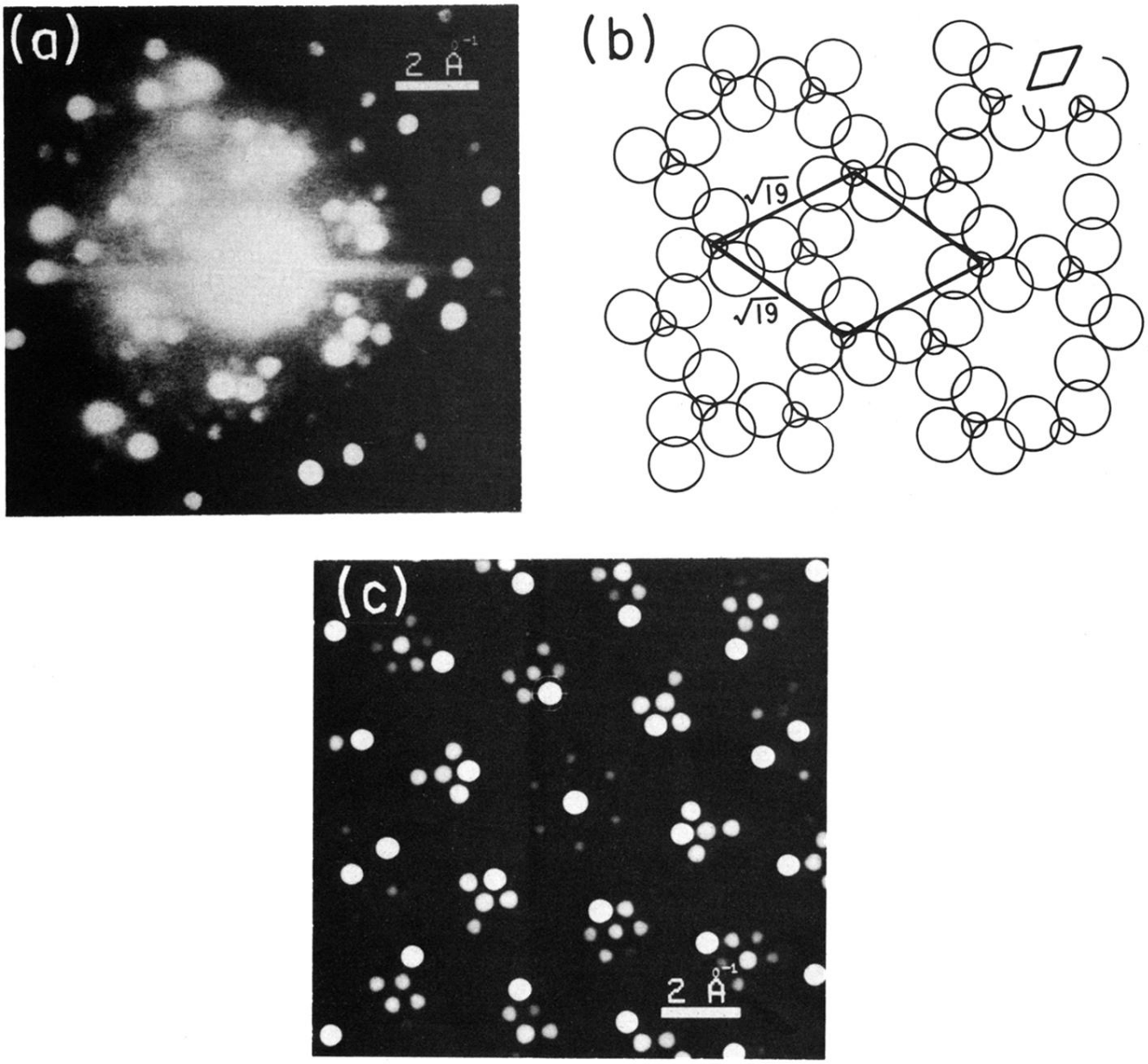

FIG. 7. (a) Diffraction micrograph from stage-4 $SbCl_5$ intercalated graphite (full scale ± 6.4 Å^{-1}). (b) Possible intercalant superlattice to explain (a). The lattice is a $(\sqrt{19}\times\sqrt{19})R23.4°$ from the graphite lattice with two molecules per unit cell. A graphite unit cell is shown in the inset at the upper right-hand corner. (c) Computer simulation of the diffraction micrograph which would be produced by the superlattice of (b). A first-order graphite spot (2.95 Å^{-1}) has been circled above and to the left of the central spot.